AIAA JOURNAL
Vol. 42, No. 5, May 2004

Aerodynamic and Structural Resonance of an Elastic Airfoil Due to Oncoming Vortices

K. F. Luk*
Hong Kong University of Science and Technology, Hong Kong, People's Republic of China
R. M. C. So,† R. C. K. Leung,‡ and Y. L. Lau§
Hong Kong Polytechnic University, Hong Kong, People's Republic of China
and
S. C. Kot¶
Hong Kong University of Science and Technology, Hong Kong, People's Republic of China

Aerodynamic and structural resonance of an elastic airfoil in a uniform stream with oncoming vortices was investigated experimentally and numerically. An experiment was designed to create two parallel rows of vortices that serve as external excitation for the symmetric airfoil (NACA 0012). The vortices were produced by two identical side-by-side circular cylinders of diameter D in a uniform stream located at a fixed distance ahead of the airfoil. The whole arrangement was placed symmetrically about the midplane in the test section of a wind tunnel. Reynolds numbers ranging from $\sim 8 \times 10^4$ to $\sim 2 \times 10^5$ were selected because the Strouhal number was essentially constant in this range. A range of D was selected to provide a corresponding range of shedding frequencies f_s that could lead to both aerodynamic and structural resonance of the airfoil. A hot-wire anemometer and a dual-beam laser vibrometer were used to measure the wake pattern and the vortex convection velocity, and the airfoil response, respectively. The airfoil displacement amplitude at structural resonance increases by many fold compared to its value far away from resonance and the airfoil goes into a limit-cycle oscillation behavior. As D decreases, near-aerodynamic resonance is also observed. These results were used to verify a boundary element method (BEM) developed to treat vortex–airfoil interaction problems. Aerodynamic and structural resonance of an elastic airfoil in a uniform stream with oncoming vortices was correctly replicated by the BEM, thus showing that the BEM model is appropriate for fluid–structure interaction problems.

I. Introduction

AN UNDERSTANDING of turbine blade failure due to flutter and forced vibrations is of fundamental importance to the design of turbomachines and their operations. Flutter occurs as a result of self-excited oscillations created by blades extracting energy from a uniform stream.[1] On the other hand, externally applied forces and/or flow-induced forces created by nonuniformities in the flowfield (such as vortices shed from an upstream blade row) will give rise to forced vibrations of the blades. For turbine blades in a turbomachinery environment, the blades are subject to both flutter and forced-induced vibrations with nonuniformities in the flow derived from several sources: the wake in the preceding blade row, combustion or burner distortions, struts, bleeding slots and ports, and so on. When the frequencies of the external and/or flow-induced forces are close to the structural modes of blade vibration, resonance could result.[2] In this case, the blade dissipates energy into the flow and this could lead to catastrophic consequence in the turbomachine.[3] Considerable effort has been made in the past to study flutter, and this gave rise to a fairly good understanding of the flutter problem.[4,5] However, the same cannot be said about the forced-vibration phenomenon. This problem is complicated by the fluid–blade interactions, which affect the fluid–blade system damping and the modal characteristics of vibrations.

A time marching technique has been used to analyze fluid–blade interactions in a uniform flow with and without constant vorticity.[5] The analysis reveals that flutter does not lead to drastic failure; instead the blade would go into limit-cycle oscillation (LCO) whose amplitude depends to a large extent on structural nonlinearity. The case where two parallel rows of alternating vortices are superposed on the uniform flow has been numerically investigated by So et al.[6] where free and forced vibration of the blade are examined simultaneously. They found that under certain conditions, depending on the ratio of the blade chord length c and the vortex separation distance d, aerodynamic resonance could result aside from structural resonance where the frequency of the oncoming vortices is close or equal to the natural frequency of the blade. In their theoretical model, they assumed that the vortices of the top and bottom row are released at distance of $d/2$ apart, thus ensuring that the alternating vortices are always separated by $d/2$. A boundary element method (BEM) was used to carry out the analysis where the uniform flow was superposed with discrete vortices. The method has been verified against the flutter calculations of Hall[4] but not against actual measurements of blade aerodynamic and structural response in a uniform flow with alternating vortices.

The BEM analysis of So et al.[6] compared the flow-induced vibration responses of a NACA 0012 airfoil and a high-loading T1 turbine blade with no twist. Their BEM results reveal that aerodynamic and structural resonance occurs at identical resonant c/d ratios, regardless of the profile geometry and mean aerodynamic loading of the blade. This suggests that their predictions are applicable to different blade profiles at various angles of attack along the span of the blade. In an actual turbine blade disk, the blade is twisted and surrounded by a number of neighboring blades. The results of a single-blade analysis may not sufficiently represent the fluid–blade interactions in a cascade where the occurrence of aerodynamic and structural

Received 4 May 2003; revision received 18 November 2003; accepted for publication 18 December 2003.

*M.Phil. Candidate, Department of Mechanical Engineering, Clear Water Bay, Kowloon.
†Chair Professor and Head, Department of Mechanical Engineering, Hung Hom, Kowloon. Fellow AIAA.
‡Assistant Professor, Department of Mechanical Engineering, Hung Hom, Kowloon. Member AIAA.
§Ph.D. Candidate, Department of Mechanical Engineering, Hung Hom, Kowloon.
¶Senior Lecturer, Department of Mechanical Engineering, Clear Water Bay, Kowloon.

resonance may depend on the combination of c/d and blade pitch. However, from the point of view of the central blade, the presence of the neighboring blades may be considered a different boundary condition for the BEM analysis of the forced-vibration problem. Therefore, once the BEM results of forced vibration in free space are verified, the analysis can be readily extended to study fluid–blade interactions in a cascade. This has been carried out by Lau et al.[7] The effect of twist has to be dealt with in a three-dimensional formulation of the problem and cannot be treated in a two-dimensional approach.

The aim of this work is to devise an experiment to investigate the aerodynamic and structural response of a single blade subject to the passage of two parallel rows of vortices superposed on a uniform stream where the vortex release separation distance is not necessarily equal to $d/2$. Therefore, the objectives of this experiment are twofold: the first is to explore the effect of this separation distance on the blade aerodynamic response, and the second is to validate the BEM. According to So et al.,[6] aerodynamic resonance will occur when $c/d = 0.5, 1.5, 2.5$, and so forth, assuming the vortex release separation distance is $d/2$. The vortex separation distance d is related to the vortex convection velocity U_c and its frequency of release f_r by $d = U_c/f_r$. If d were to be varied in the experiment, this means that U_c/f_r has to vary by either changing U_c or f_r or both. One way to do this is to place the blade behind a circular cylinder where the frequency of the shed vortices f_s can be varied by changing the freestream velocity. In this case, f_r will be identical to f_s and the release separation distance is $d/2$. Another way is to symmetrically place a blade behind two side-by-side cylinders and to change cylinder diameter D or freestream velocity U_∞ to achieve a variation in f_s. In this case, the vortex release separation distance could vary from zero to a finite value (not necessarily $d/2$) provided the vortex streets behind the two cylinders are not synchronized.

When a cylinder is exposed to a crossflow, a Kármán vortex street (KVS) with alternating vortices is formed and shed behind the cylindrical body. The reduced frequency of vortex shedding, or Strouhal number $Sr = f_s D/U_\infty$, has been studied over a broad range of Reynolds numbers, $Re = U_\infty D/\nu$, from approximately 50 to 10^6 and even higher,[8] where ν is the fluid kinematic viscosity. Furthermore, the mechanics of vortex formation has been closely examined by numerous researchers using hot-wire anemometry, flow visualization, and numerical modeling.[9–11] It is generally agreed that the vortex formation region has an important role in vortex shedding and its frequency f_s. Roshko[12] showed that f_s increased when the scaled formation region was reduced. On the other hand, Nakagawa et al.[13] found that decreasing the area of the vortex formation region could lead to an increase in f_s and vice versa. It has also been shown by Roshko[12] and Gerrard[14] that f_s was modified when a splitter plate was placed in the near-wake region. This arrangement, in essence, varies the length of the vortex formation region. There is no common definition for the vortex formation region. Some researchers defined it as the distance between the cylinder and the maximum of the wake velocity fluctuation at twice f_s. Other definitions[12,14,15–17] were based on the distance between the cylinder and the minimum of the mean pressure on the wake axis, or the distance between the cylinder and the maximum of the wake velocity fluctuation at the fundamental shedding frequency.

These studies have shown that it is possible to vary f_s by controlling the vortex formation region. Numerous methods have been proposed based on this understanding to reduce the effect of vortex-induced vibrations. Splitter plate, spoiler plates, helical strake, and periodic rotation of the cylinder are some of the more commonly used passive control methods.[2] Besides, numerous studies have also been carried out on a cylinder/splitter plate arrangement to investigate the effect of the splitter plate on Sr. For example, Ozono[18] conducted an experiment similar to that of Roshko[12] in which a splitter plate was placed at a gap distance S behind a circular cylinder and at Re ranging from 6.7×10^3 to 2.5×10^4. It was found that when the gap distance was decreased to a critical length, both the base suction pressure coefficient and Sr decreased rapidly and increased again slightly when the gap was decreased beyond this critical length. This phenomenon could be attributed to the elongation of the vortex formation length behind the cylinder. A similar result has also been observed by Hasan and Budair[19] on square and circular cylinders.

Nakagawa et al.[20] replaced the thin splitter plate with a slender airfoil and discussed how the vortex shedding process was influenced by the spacing between the square cylinder and the downstream airfoil in the Re range of 0.7×10^5 to 3×10^5. Besides observing a jump in Sr at the critical length, flow visualization also revealed that when the airfoil was at or within the critical length the separating shear layers from the upstream square cylinder reattached to the downstream airfoil. Once the spacing became greater than the critical value, the airfoil did not have any significant effect on the vortex shedding process of the square cylinder. The dynamic response of a symmetric airfoil behind a single cylinder has been investigated experimentally and numerically using BEM.[21] In this experimental setup, the vortex release and alternating vortex separation distance is $d/2$ as stipulated in the model of So et al.[6] Good agreement between model predictions and measurements was obtained.

Parallel rows of vortices can be generated by considering the flow around two cylinders in a side-by-side arrangement. The behavior of this type of flow has been investigated extensively in the past.[22] Most of the work concentrates on examining the interference between cylinders and its effect on the mean drag and lift. Studies on vortex formation and the wake pattern have been carried out by Landweber,[23] who observed a single vortex street for $T/D \leq 1.5$ and two distinct vortex streets for $T/D > 2$, where T is the separation distance measured between centers of the cylinders. Similar findings were obtained by Spivac,[24] who measured two different frequencies in the wake for $T/D < 2$ and a single frequency for $T/D > 2$. Flow visualization of the wake behind two side-by-side cylinders using a schlieren optical method[25] revealed symmetric vortex formation and shedding for $T/D = 2.5$ and 3.0 but a biased gap flow for $1.5 < T/D < 2$. Together, these studies show that two separate KVSs with the same shedding frequency are formed behind two cylinders in a side-by-side arrangement if $T/D \geq 3$. Again, f_s can be varied by changing D or U_∞.

Ideally, the KVSs shed from two side-by-side cylinders with $T/D \geq 3$ are in phase, have a single f_s, and are aligned in the vertical direction. The KVS shed from the top cylinder is denoted as KVS1 and that below as KVS2. Assuming this ideal situation to be true, the vortices from the two KVSs would impinge on the blade simultaneously at the same chord location on its top and bottom side, thus canceling the effect of vortex impingement if the blade is symmetrically placed between the two KVSs. Because vortex shedding is an unsteady phenomenon, the shedding process is affected by numerous factors. Some of these are related to cylinder surface finish, steadiness of the approaching stream, behavior of the front stagnation regions, and freestream turbulence. Therefore, the two KVSs are most likely not completely synchronized. The lack of synchronization will result in a time lag between KVS1 and KVS2, and this will translate into a separation distance x_r between the starting vortices shed from the bottom row of KVS1 and the top row of KVS2. It is anticipated that x_r, no matter how small, could change the dynamic response of the blade. Therefore, an experiment with c, S, and T fixed could be carried out to investigate the effect of x_r on blade response with x_r and f_s varying. The latter can be varied by changing D whereas the variation of x_r is a function of the aerodynamics around the two side-by-side cylinders.

II. Experimental Details

From the preceding discussion, it is clear that two side-by-side cylinders would be an appropriate setup used to generate two parallel rows of vortices to replicate the theoretical conditions.[6] Therefore, an experiment was designed with an airfoil to represent the blade placed symmetrically behind two identical cylinders in a side-by-side arrangement in a crossflow at $T/D \geq 3$ to investigate the aerodynamic and structural response of the airfoil. The oscillation of the airfoil derived from the shed vortices of the upstream cylinders can be examined in detail by varying D and, hence, f_s. The vibration induced on the airfoil would be very small in airflow. Therefore, it could be argued that the experiment would not be able to provide useful data on airfoil vibration even if the airfoil structural

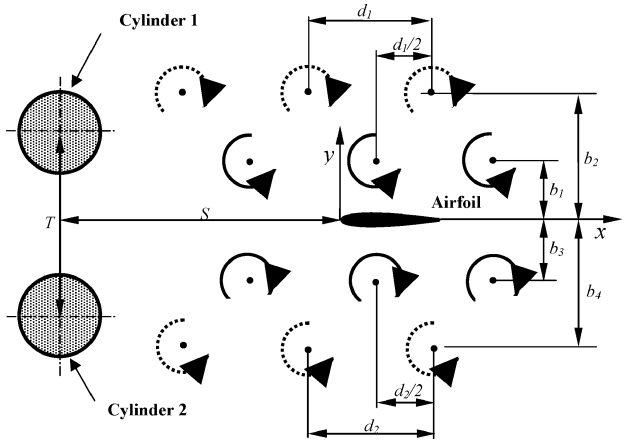

Fig. 1 Schematic diagram of the two coupled side-by-side circular cylinders/airfoil system.

property is selected to give as small a finite stiffness as possible. However, modern optical diagnostic techniques are able to resolve vibration amplitude accurately down to 10^{-5} m. Once measured, the displacement signals can be used to extract frequency and damping ratio information[26] concerning the interaction phenomenon and the possible occurrence of resonance. The data thus obtained could be used to verify the BEM. Details of the experimental setup and measurement techniques are briefly described in the following sections.

A. Wind-Tunnel Setup

A schematic diagram of the cylinder/airfoil setup in the wind tunnel is shown in Fig. 1, where the cylinder/airfoil assembly was symmetrically placed along the midplane of the test section of the CLP Wind Tunnel Facility of the Hong Kong University of Science and Technology. The overall dimensions of the tunnel are 61.5 m long, 16.5 m wide, and 7.5 m high. There are two major sections, a low-speed section and a high-speed section. The experiment was set up in the high-speed-section area behind a contracting section where the turbulence intensity and wall boundary-layer thickness were relatively small. The test section has a cross section 3 m wide, 1.8 m high, and 2 m long. The section was partitioned to 590 mm height to fit the test model. The turbulence intensity in the central core of the test section was measured to be approximately 0.2% over the range of freestream velocity tested. Therefore, the freestream turbulence effect on the aerodynamic and structural response of the airfoil is minimal. The velocity in the test section was controlled by adjusting the fan speed, and the maximum velocity was approximately 33 m/s. In the present experiment, the freestream velocity U_∞ was fixed at 30.3 m/s, thus giving a Re range of 7.7×10^4 to 2.05×10^5 based on D.

B. Vortex Generators

Two identical hollow circular cylinders with outer diameter D were used to generate the alternating vortices upstream of the airfoil. The cylinders were fixed mounted at both ends and in side-by-side arrangement with a fixed separation $T = 0.305$ m, where T was measured from center to center. From Fig. 1, it can be seen that, given a fixed configuration and a constant U_∞, the parameters f_s, b_1, b_2, b_3, b_4, d, and Γ are fixed for a given D. The vortex separation distances in the x and y directions are given by d and b_1, b_2, b_3, b_4, respectively, where the x axis is taken to be the symmetry axis of the side-by-side cylinders and y is the normal coordinate. The origin of x and y is set at the leading edge of the airfoil. The vortex strength Γ and d are not independent and they are set once D is chosen. Setting T equal to a constant has its advantage. In the course of the experiments, it was found that keeping T constant at $T/D \geq 3$ would allow the distance between the airfoil and its closest rows of vortices to become approximately constant (i.e., $b_1 = b_3 =$ constant), thus minimizing the effect of the distance between vortex and airfoil and helping to eliminate this variable as another parameter that could affect the airfoil response to vortex impingement. This way, the two parallel rows of vortices specified in the analysis of So et al.[6] can be duplicated and the parameter c/d could be varied by changing D.

Table 1 Properties of the airfoil

Quantity	Notation	Value
Chord length	c	0.2 m
Span	b	0.5 m
Centroid	——	$0.42c$
Shear center	——	$0.37c$
Material	——	Polyurethane
Density	ρ	770 kg/m^3
Mass	m	1.3 kg
Mass ratio	m^*	640
Mass moment of inertia	I	0.00284 kgm^2
Bending stiffness	EI	66.5 Nm^2
Torsion stiffness	GJ	114 Nm^2
Natural frequency in vacuo: bending	f_b	73 Hz
Natural frequency in vacuo: torsion	f_θ	200 Hz
Damping ratio: bending	ζ_b	0.016
Damping ratio: torsion	ζ_θ	0.021

The cylinders have a wall thickness of 1.59 mm and a diameter D that varied from 38.1 to 101.6 mm (Table 1). This choice of D was selected to approximately give $b_1 = b_3$. Blockage due to the largest cylinder was estimated to be 3.4%. Therefore, tunnel blockage effect on the mean drag and vortex shedding could be considered minimal and no corrections were made in the experiments.[27] Various properties of the cylinders were summarized in Table 1. The cylinder stiffness EI varies from 1.25×10^5 Nm^2 for the largest cylinder to 2.22×10^3 Nm^2 and its corresponding natural frequency f_c from 1825 to 686 Hz. The natural frequency was determined from impact tests conducted in still air. The reduced velocity U_r was calculated to vary from 0.163 to 1.16. If a two-degree-of-freedom (2-DOF) structural dynamics model is assumed for the cylinder vibration at its midspan, it can be shown that the normalized equation of motion would lead to negligibly small displacement amplitude when U_r is very small.[2,28,29] Therefore, vortex-induced vibration of the cylinder is insignificant and the cylinders can be essentially considered rigid. This conclusion is further substantiated if the natural bending frequencies of the cylinders and the airfoil are compared. From Tables 1 and 2, the ratio of cylinder to airfoil bending frequency is calculated to vary from 9.4 to 25. This choice was built into the experimental design so that the dynamic response of the airfoil alone was investigated and the effect of cylinder vibration on the airfoil response could be reduced to a minimum.

C. Airfoil Arrangement

A symmetric NACA 0012 airfoil was chosen for this investigation. It was positioned to give a zero angle of attack with respect to the x axis and was placed at $S = 0.203$ m downstream of the two side-by-side cylinders. This separation distance was maintained constant for all experiments. Only the cylinder diameter D was varied. The chord length c and span b of the airfoil were 0.2 and 0.5 m, respectively. The centroid and shear center were located at $0.42c$ and $0.37c$, respectively, from the airfoil leading edge. To fabricate an elastic airfoil for vibration measurement, a polyurethane modeling board, with density $\rho = 770$ kg/m^3 and elastic modulus $E = 1.2$ GPa, was used to make the airfoil. The airfoil was fixed mounted at both ends in the test section, and the bending and torsion stiffness were estimated to be $EI = 66.5$ Nm^2 and $GJ = 113$ Nm^2, respectively. The natural frequencies of bending and torsion were determined to be 73 and 200 Hz, respectively, from impact tests in still air. The corresponding damping ratios were estimated to be 0.016 and 0.021. Structural properties of the airfoil are summarized in Table 2.

D. Measurement Techniques

A Polytec OFV-3001/OFV-502 dual-laser vibrometer system was used to measure the vibration of the airfoil. The bending mode vibration Y was measured by pointing a single laser beam at the midspan of the airfoil at the aerodynamic center. The torsion vibration θ was measured by pointing the laser beams at two points along the chord,

Table 2 Properties of the circular cylinders

Outer diameter D, m	Inner diameter D_i, m	Mass m_c, kg	Mass ratio m_c^*	Bending stiffness E_cI_c, N/m^2	Natural frequency in vacuo: bending $(f_{Y1})_c$, Hz	Reduced velocity $(U_r)_c$	Reynolds number Re
0.1016	0.0984	2.31	387	1.25×10^5	1825	0.16	2.05×10^5
0.0889	0.0826	3.97	866	1.57×10^5	1565	0.22	1.80×10^5
0.0762	0.0730	1.73	513	5.18×10^4	1361	0.29	1.54×10^5
0.0635	0.0603	1.43	613	2.96×10^4	1130	0.42	1.28×10^5
0.0508	0.0476	1.14	761	1.49×10^4	898	0.66	1.03×10^5
0.0381	0.0349	0.29	346	2.22×10^3	686	1.16	7.70×10^4

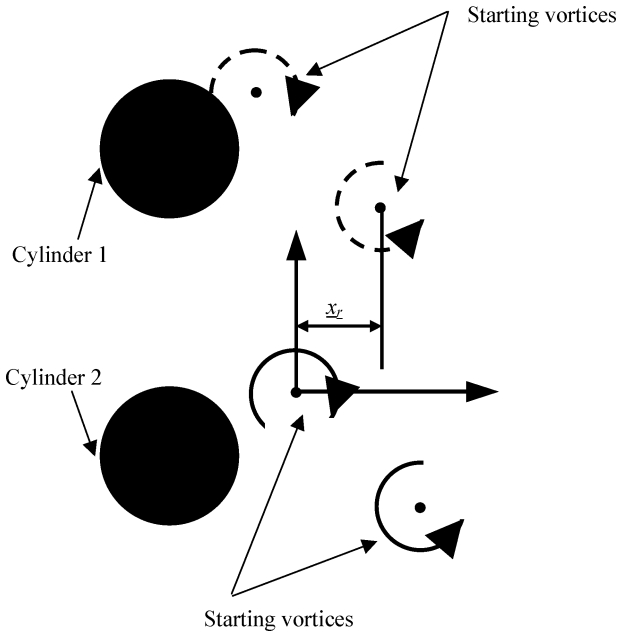

Fig. 2 Schematic showing the definition of x_r, the separation distance between the starting vortices from KVS1 and KVS2.

one at the aerodynamic center and another at 180 mm from the leading edge, which measured the differential at these two points. The vibrometer system was connected to a 12-bit A/D converter, and the sampling frequency was set at 1 kHz. The uncertainty of the measurement was estimated to be $\pm 3\%$.

The shedding frequency f_s was measured by an IFA-300 constant-temperature anemometer system using a single wire to detect the unsteady stream velocity u in the cylinder wake. The hot-wire probe was placed at $y = 170$ mm away from the leading edge of the airfoil to measure the vortex shedding frequency from the upstream cylinder. In addition, the hot wire was used to measure the separation distances of the vortices by traversing along the y direction starting from the leading edge of the airfoil. The sampling frequency was set at 1 kHz and the uncertainty in the flow velocity measurement was estimated to be less than $\pm 1\%$. Thus, knowing the shedding frequency and the vortex separation distance, the vortex convection velocity can be deduced.

Even though the vortex streets behind the identical cylinders are essentially the same, there might be a time lag between the two KVSs. This time lag will in turn lead to a separation distance x_r between the top and bottom rows of vortices in the two KVSs (Fig. 2) and can be measured by positioning two hot wires downstream of the side-by-side cylinders. The hot wires were located at $x = 180$ mm downstream of the cylinder centers and one on each side of the x axis. As for the y location, it was fixed at $y = \pm 0.45D$ and varied from one setup to another. The two hot-wire signals were recorded simultaneously and they were analyzed to determine the phase difference and the time lag. Once the time lag is known, the separation distance x_r can be determined.

The analog signal from the dual-laser vibrometer was digitized using a 12-bit A/D converter connected to a personal computer.

Table 3 Shedding frequency generated by circular cylinders of different diameters

D, m	T/D	U_∞, m/s	Re	f_s, Hz	$Sr = f_sD/U_\infty$
0.1016	3.002	30.3	2.05×10^5	54.7	0.183
0.0889	3.431	30.3	1.80×10^5	62.5	0.183
0.0762	4.003	30.3	1.54×10^5	71.3	0.182
0.0635	4.803	30.3	1.28×10^5	85.0	0.178
0.0508	6.004	30.3	1.03×10^5	108.0	0.181
0.0381	8.005	30.3	7.70×10^4	146.0	0.184

Analysis in frequency domain was carried out using conventional fast Fourier transform (FFT) software, and the spectrum resolution was estimated to be $\Delta f = 0.122$ Hz. For the hot-wire anemometer measurement, the velocity signals were analyzed using conventional FFT software with an estimated $\Delta f = 0.977$ Hz. These frequency resolutions are sufficient to allow the variation of the system natural frequencies due to fluid–structure interaction to be determined with confidence.

III. Results and Discussion

To achieve the stated objectives, the vortex pattern behind the cylinders has to be known, and the airfoil response needs to be analyzed to determine whether aerodynamic and structural resonance occur within the range of parameters investigated. Once these results are available, the vortex pattern is used as inputs to the BEM and its predictions can be compared with the measured airfoil response. Therefore, the results and discussion that follow are divided into three subheadings; namely, Vortex Pattern, Airfoil Response, and BEM Predictions.

A. Vortex Pattern

Analysis of the single hot-wire measurement at a fixed x and y location yields the shedding frequency f_s for a given U_∞ and D. This is obtained by examining the calculated velocity spectrum. The location of the dominant peak in the spectrum is the shedding frequency. Thus deduced, the results for the six different cylinders tested are given in Table 3 together with the calculated Strouhal number, $Sr = f_sD/U_\infty$. It can be seen that Sr in the Re range tested is indeed constant. The error amounts to about 2%; that is, the error in determining f_s is also about 2%.

The hot-wire traverse along the y direction in the plane of the airfoil leading edge is used to deduce b_i and the vortex convection velocity U_c. Only the u component of the velocity vector was measured. Plots of the mean velocity U for the six different D tested are shown in Fig. 3, and plots of the root mean square u, $u_{\rm rms}$, are given in Fig. 4. The origin of Figs. 3 and 4 represents the location of the leading edge of the airfoil. If the center of the vortex is taken to be the location where $u_{\rm rms}$ is a maximum, then the time-averaged position of the alternating vortices for a given D can be determined from Fig. 4. The corresponding distance along the horizontal axis of Fig. 4 represents the distance between each row of vortex and the airfoil. With these locations known, the velocity at these corresponding locations is the convection velocity of the vortices U_c for a particular D. Ideally, U_c should be the same for KVS1 and KVS2. Only U_c of the bottom row of KVS1 and the top row of KVS2 are evaluated. Once U_c is known, $d = U_c/f_s$ can be determined. These

Table 4 Properties of the two rows of vortices passing by the airfoil

D, m	U_{c1}/U_∞	U_{c2}/U_∞	U_{cm}/U_∞	c/d_1	c/d_2	c/d_m	$b_1/c, b_3/c$	$b_2/c, b_4/c$	$x_r/d_m = \chi/2\pi$	$\Gamma/U_\infty c$
0.1016	0.716	0.639	0.678	0.504	0.565	0.535	0.735	1.495	0.2055	0.480
0.0889	0.681	0.671	0.676	0.606	0.615	0.611	0.735	1.400	−0.0223	0.574
0.0762	0.688	0.634	0.661	0.684	0.742	0.713	0.735	1.305	0.0302	0.689
0.0635	0.709	0.664	0.687	0.791	0.845	0.818	0.730	1.205	−0.2338	0.767
0.0508	0.712	0.655	0.684	1.001	1.088	1.045	0.735	1.112	0.0408	0.863
0.0381	0.731	0.713	0.722	1.318	1.352	1.335	0.750	1.025	0.1040	0.990

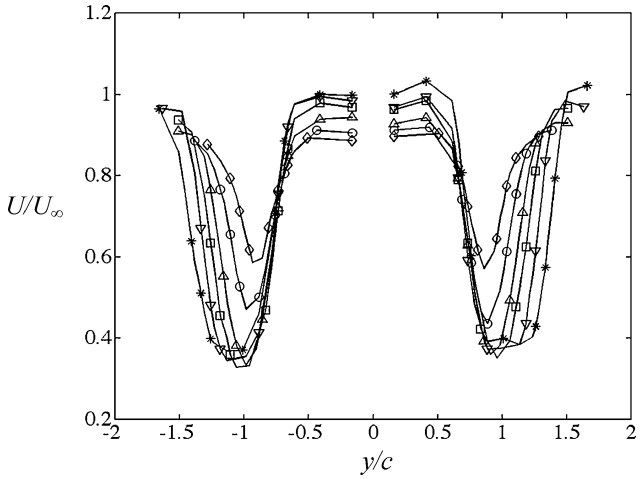

Fig. 3 Variation of the mean velocity U behind the side-by-side cylinders in the y direction: ◇, $D = 38.1$ mm; ○, $D = 50.8$ mm; △, $D = 63.5$ mm; □, $D = 76.2$ mm; ▽, $D = 88.9$ mm; ∗, $D = 101.6$ mm.

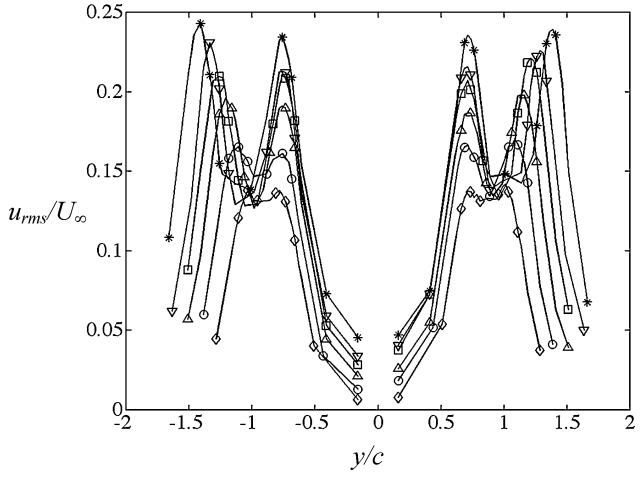

Fig. 4 Variation of turbulence intensity ($u_{\rm rms}/U_\infty$) behind the side-by-side cylinders in the y direction: ◇, $D = 38.1$ mm; ○, $D = 50.8$ mm; △, $D = 63.5$ mm; □, $D = 76.2$ mm; ▽, $D = 88.9$ mm; ∗, $D = 101.6$ mm.

results are tabulated in Table 4 for reference and for use as inputs to the BEM calculation. In Table 4, U_c is labeled with a subscript 1 or 2 to indicate whether it is determined from KVS1 or KVS2, respectively. Similarly, the corresponding subscript in d also denotes the vortex separation distance of KVS1 and KVS2. It can be seen that $b_1/c = b_3/c = 0.735$ and the value is essentially constant for the six cases tested. In other words, the design objective of the test model has been accomplished. Furthermore, it shows that the cylinders are far enough apart not to have any influence on the wake pattern of the neighboring cylinder. The c/d ratio is not identical for the two KVSs for the six cases tested. The difference varies from about 2% for the smallest cylinders to about 10% for the largest cylinders. For the sake of calculations, the average of d_1 and d_2 can be specified as the input d_m for the BEM. Once these parameters are known, they can be used as inputs to the KVS theory to determine Γ (Ref. 30).

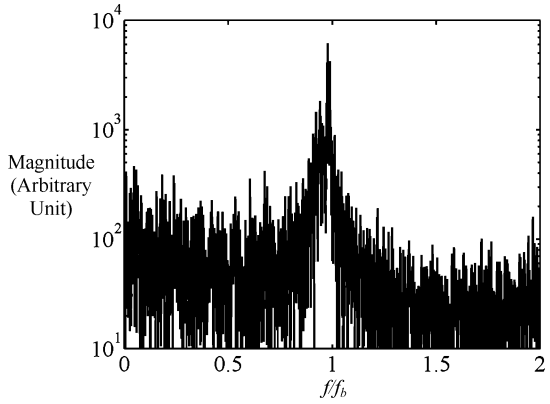

Fig. 5 Cross spectrum of the two u velocity measurements behind the cylinders with $D = 0.0762$ and $f_s = 71.3$ Hz.

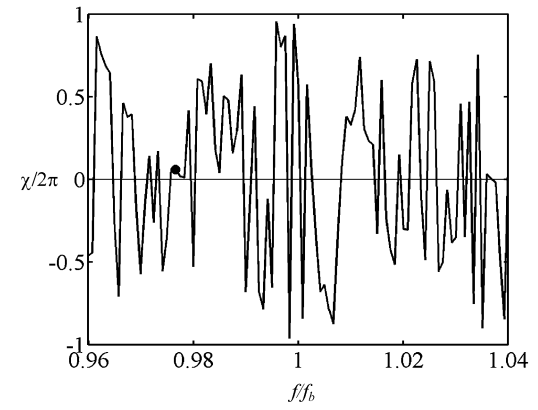

Fig. 6 Phase plot of the two velocity signals behind the side-by-side cylinders with $D = 0.0762$ and $f_s = 71.3$ Hz in a narrow range of f/f_b.

The values of Γ thus determined are listed in Table 4 as $\Gamma/U_\infty c$. It can be seen that the smallest cylinders give the strongest circulation for the shed vortices.

The position of the starting vortices is also required as an input to the BEM. In the present case, this is equivalent to evaluating x_r, the vortex release separation distance between the top and bottom KVSs. This can be determined from the equation $x_r = \chi d/2\pi$, where χ is the phase difference between the velocity signals evaluated at f_s. The velocity signals were measured by the two hot wires located downstream of the cylinders and symmetrically placed about the x axis. This phase difference can be deduced from the cross-spectral-density plots calculated from the two hot-wire signals using MATLAB. In all calculations, the signal from the hot wire located behind cylinder 2 is used as a reference. A plot of the cross spectrum for the case where $D = 0.0762$ m and $f_s = 71.3$ Hz (Table 4) is shown in Fig. 5. The frequency axis in this figure is normalized by f_b. The two velocity signals are highly correlated around f_s because it is essentially equal to f_b. A magnified phase plot around $f_s/f_b = 1$ is shown in Fig. 6 to identify the correct phase lead (or lag) $\chi/2\pi$ at f_s; thus determined, it is used to calculate x_r. The results of $x_r/d_m = \chi/2\pi$ are also listed in Table 4.

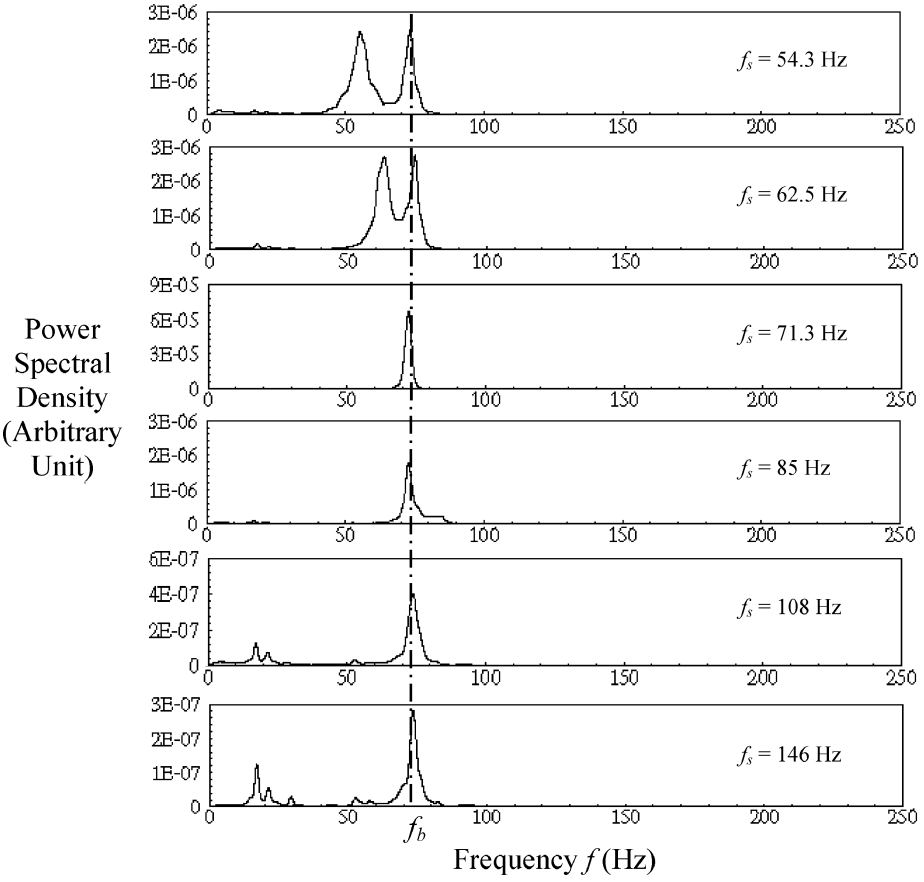

Fig. 7 Power spectral density plots of Y of the airfoil at different f_s.

It is obvious that the KVSs shed from cylinders 1 and 2 are independent of each other and are essentially the same for all D and Re tested. However, the two KVSs are not synchronized and there is a time lead (or lag) between the two. The resulting vortex separation distance thus determined essentially defines the release position of the starting vortices and forms a part of the inputs for the BEM calculation.

B. Airfoil Response

The measured plunging displacement Y and pitching angle θ time series are analyzed using MATLAB. From the analysis, the power spectral density plots (Figs. 7 and 8), the root mean square values $(Y/c)_{\text{rms}}$ and θ_{rms} (Figs. 9 and 10), and the energy content of the power spectral density plots (Fig. 11) are deduced. It can be seen from the power spectral density plots of Y that the airfoil was excited at f_b only, the natural bending frequency of the airfoil, when the shedding (or vortex excitation) frequency f_s was near or greater than f_b. As the excitation frequency f_s decreases below f_b, another peak begins to emerge in the power spectral plots. This peak becomes very prominent when f_s is reduced to 62.5 Hz and is even more so when $f_s = 54.3$ Hz. From Table 4, it can be seen that c/d for the two KVSs shows a declining value as f_s decreases even though it is different for KVS1 and KVS2. Consequently, the airfoil sees two parallel rows of vortices with two different values of d. The normalized c/d for the top row is $c/d_1 = 0.504$ and that for the bottom row is $c/d_2 = 0.565$ for the case where $f_s = 54.7$ Hz. Nevertheless, the approach to aerodynamic resonance, where $c/d = 0.5$ as predicted by the model of So et al.,[6] is slowly realized. Therefore, the second peak in the power spectral density plots of Y (Fig. 7) can be said to represent the near-aerodynamic resonance response of the airfoil under the conditions set up in the experiment. There is another peak occurring at around $f = 18$ Hz for the two cases where $f_s = 108$ and 146 Hz. This low-frequency contribution is most likely coming from wind-tunnel wall vibration due to the axial flow fan. Another indication of near resonance can be gleaned from the phase plane plots of Y. The plot for the case where $f_s = 54.7$ Hz is shown in Fig. 12. The circular behavior of the plot indicates LCO, a fact consistent with the analysis of So et al.[6] For true resonance, the phase plane plot would show only one circle. The multiple circles indicate that it is near resonance.

The power spectral density plots of θ show multiple peaks, one at f_b, another at f_θ, and a relatively more prominent one at $f = 54.7$ Hz (Fig. 8). For the $f_s = 71.3$ Hz case, there is only one peak and that occurs at f_b. Because the excitation frequency for this case is very close to $f_b = 73$ Hz, structural resonance occurs. This is why all other responses are not evident relative to the structural resonance response in the power spectral density plot, not even that at $f_\theta = 200$ Hz. For the $f_s = 54.7$ Hz case, a relatively more prominent peak is noticed at $f = 54.7$ Hz, which is further evidence that a near-aerodynamic resonance response is occurring at this frequency. The response at the excitation frequency is evident in Fig. 8 for all other cases; however, the peak is not as prominent as that for the $f_s = 54.7$ Hz case. From Figs. 7 and 8, it can be observed that the pitching effect on the plunging response is essentially nonexistent, but the same is not true for the effect of plunging on the pitching response. Again, the peaks noted in the region $f \leq 20$ Hz could be attributed to tunnel-wall vibration.

The occurrence of structural and near-aerodynamic resonance is further supported by examining the distribution of $(Y/c)_{\text{rms}}$ and θ_{rms} vs f/f_b. These plots are given in Figs. 9 and 10, respectively. Two peaks are observed in these two figures, one at $f/f_b \approx 1$ and another at $f/f_b \approx 0.75$. These two peaks correspond to structural and near-aerodynamic resonance of the airfoil. Finally, a plot of the energy content of the spectra, obtained by integrating the area under the power spectral density plots, is shown in Fig. 11. Clearly, there is a large jump at $f/f_b \approx 1$ and a smaller increase at $f/f_b \approx 0.75$. This is further evidence that true aerodynamic resonance has not quite been reached yet.

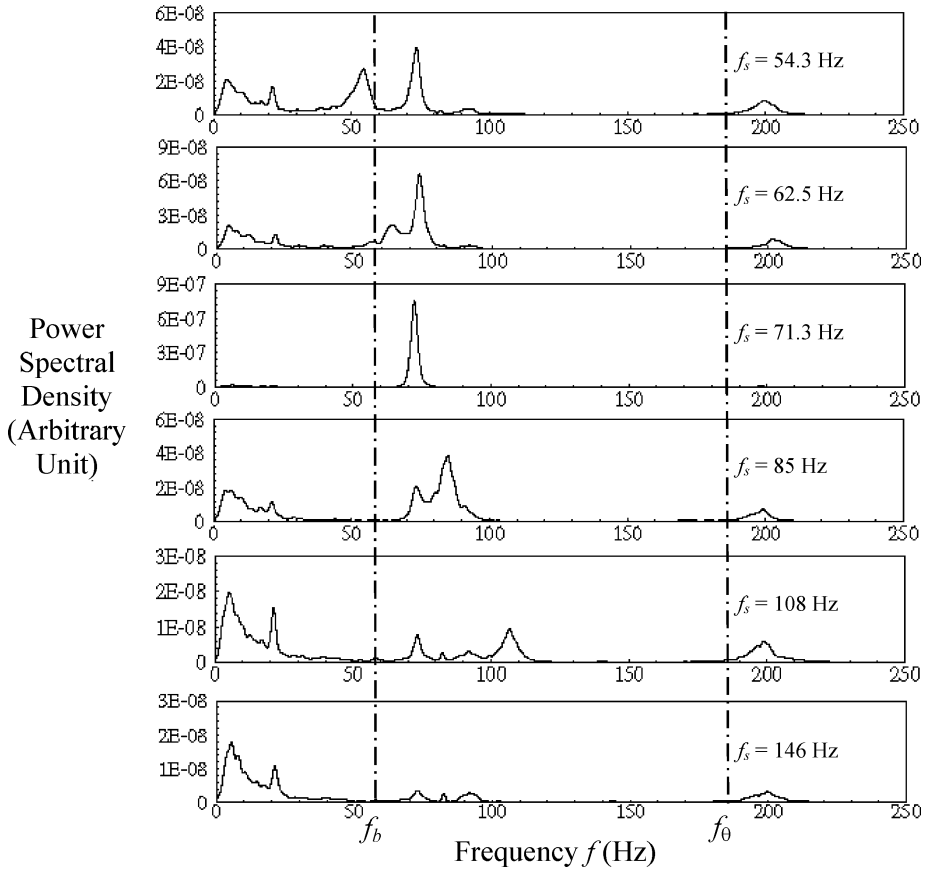

Fig. 8 Power spectral density plots of θ of the airfoil at different f_s.

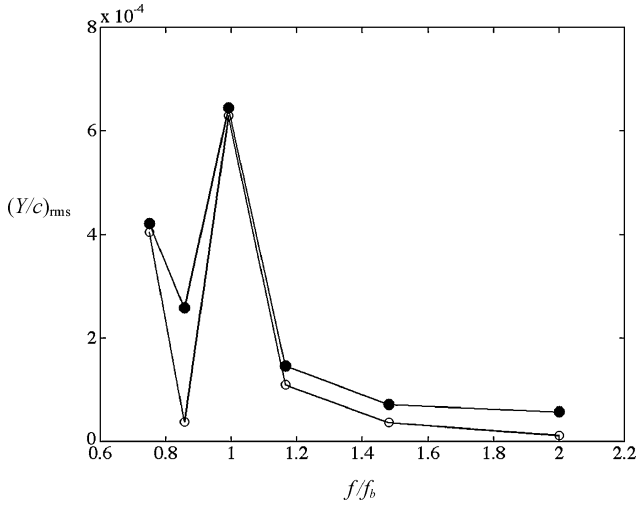

Fig. 9 Variation of $(Y/c)_{rms}$ with f/f_b: ●, experimental data and ○, BEM predictions.

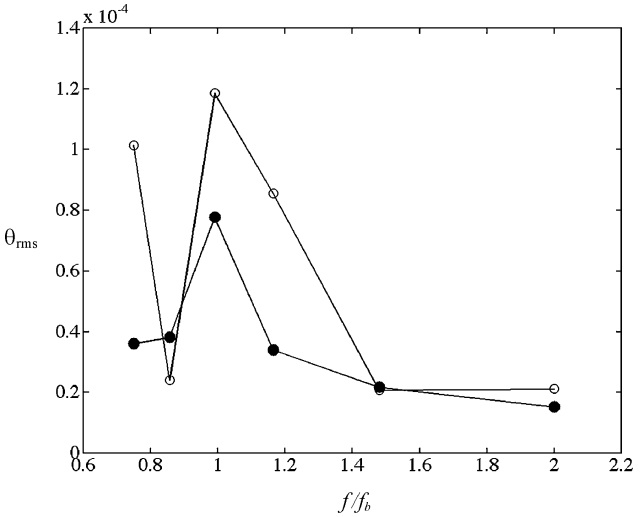

Fig. 10 Variation of θ_{rms} with f/f_b: ●, experimental data and ○, BEM predictions.

C. BEM Predictions

In considering fluid–structure interaction problems, three calculation areas are of concern. The first is the flowfield calculation, the second is the structural dynamic calculation, and the third is the consideration of the fluid–structure interaction whereby the changing boundary conditions due to the motion of the structure are fully accounted for in the calculation of the flow and, in turn, the changing aerodynamic loading on the structure is taken into account in the solution of the structural dynamic equations. A time marching technique to treat this problem has been proposed by Jadic et al.[5] and has been used by So et al.[6] to calculate fluid–blade interaction with oncoming vortices in the freestream. The technique simulated the structure using sources and vortices, solved the vorticity transport equation using the method of fractional steps,[31] and assumed a 2-DOF model for the structural dynamics.

In the flowfield calculation, the flow is assumed to be inviscid and incompressible. Therefore, the starting point of the technique is the unsteady vorticity ($\omega = \nabla \times \boldsymbol{V}$) equation, which can be derived by taking the curl of the Euler equation. The vortices in the flow can be assumed to be conveyed by the inviscid flow with the vorticity frozen while conveying. In other words, the circulation Γ around a given material curve is taken to remain constant during a time step δt. In mathematical terms, it can be expressed as

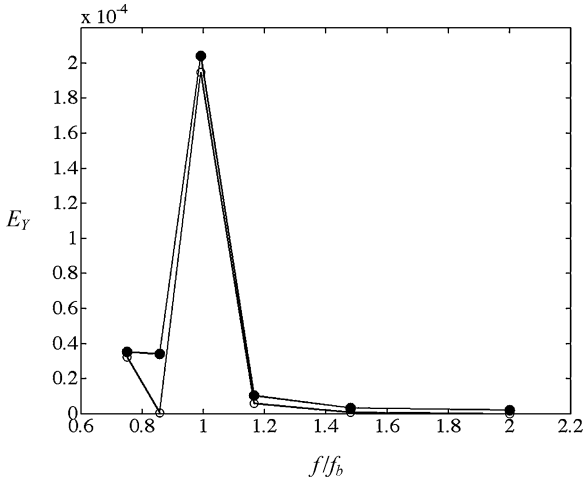

Fig. 11 Variation of bending energy E_Y of the airfoil with f/f_b: ●, experimental data and ○, BEM predictions.

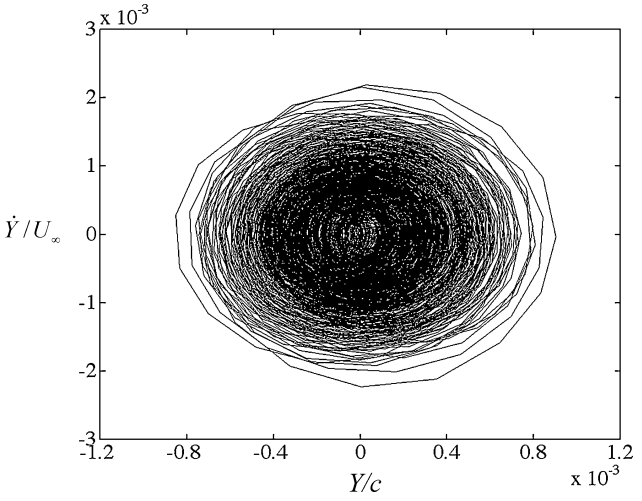

Fig. 12 Phase plane plot of the bending response of the airfoil under vortex-induced excitation at $f_s = 54.7$ Hz.

$$\boldsymbol{x}_i^v(t+\delta t) = \boldsymbol{x}_i^v(t) + \boldsymbol{V}_0\left[\boldsymbol{x}_i^v(t), \omega_i(t)t\right]\delta t, \qquad i = 1, 2, \ldots, N \tag{1}$$

where $\omega_i(t)$ is the strength of the ith vortical element, $x_i^v(t)$ is the position vector of the ith vortical element, N is the number of vertical elements, and $\boldsymbol{V}_0$ is the convective velocity. Here, a boldface letter is used to represent vector. The set of Eq. (1) is an explicit finite difference form of the differential set of equations that track the position of a certain vertical element to the velocity of the inviscid flow at that particular position. A distribution of sources and discrete vortices can be used to simulate the flow around the structure. The boundary condition requires the flow to be tangent to the surface of the structure and the far-field velocity is given by $\boldsymbol{V}_0 = \boldsymbol{V}_\infty + \boldsymbol{V}_\omega$, where $\boldsymbol{V}_\omega$ is the rotational part of $\boldsymbol{V}_0$ and $\boldsymbol{V}_\infty$ is the freestream velocity. In the present study, $\boldsymbol{V}_\infty$ is assumed to be represented by $\boldsymbol{i}U_\infty$, where $\boldsymbol{i}$ is taken to be the unit vector along the x axis. The BEM is used to solve the boundary equations, which yield the distribution of sources and vortices on the structure surface. Then, successively, the flow velocities and pressure distributions are calculated.[32] Once the unsteady velocity and pressure field, $\boldsymbol{V}$ and p, respectively, are known, the unsteady forces on the structure can be determined by integrating the surface pressure around the structure. In this formulation, the flow is attached to the structure surface and a free-wake model is assumed.[33]

The dynamic response of the structure is governed by a set of ordinary differential equations if the structure is approximated by lumped masses. However, if a 2-DOF model is assumed, the dynamic equations for the airfoil/blade can be written as

$$m\ddot{Y} - ma\cos\theta(\ddot{\theta}) + k_Y Y + ma\sin\theta(\dot{\theta}^2) = L \tag{2}$$

$$I\ddot{\theta} - ma\cos\theta(\ddot{Y}) + k_\theta\theta = M \tag{3}$$

where L and M are the unsteady lift and moment acting on the airfoil/blade, m is the mass of the airfoil/blade section per unit spanwise length, I is the moment of inertia of the airfoil/blade section, and k_Y and k_θ are the bending and torsional stiffness. If the pitching angle is small, $\cos\theta \approx 1$ and $\sin\theta \approx 0$, and Eqs. (2) and (3) can be reduced further.

Finally, fluid–structure interaction is accounted for through iteration at each time step of the flowfield and structural dynamic calculations until the solution of the flow governing equations and the 2-DOF model equations converge to a prescribed accuracy. Details of this technique have been given previously[5,6]; interested readers can see Refs. 5 and 6.

The present problem is as specified in Figs. 1 and 2. If the BEM is used to analyze this problem, c/d, x_r/d, and $\Gamma/U_\infty c$ need to be specified. These parameters have been deduced from the measured wake pattern behind the two side-by-side cylinders and are listed in Table 2. Because the two KVSs are not exactly identical, the vortex separation distance d of the two KVSs is not the same. For the purpose of the BEM calculation, a mean value d_m deduced from the measured d of KVS1 and KVS2 is assumed. Therefore, the values c/d_m, x_r/d_m, and $\Gamma/U_\infty c$ listed in Table 2 are used as inputs for the BEM. Calculations are carried out for the six cases investigated experimentally and the results of $(Y/c)_{\rm rms}$, $\theta_{\rm rms}$, and E_Y are also plotted in Figs. 9–11 for comparison with experimental data. Considering the fact that d is not the same for the top and bottom rows of vortices passing the airfoil and a mean d has to be specified instead, the agreement between measurements and predictions of $(Y/c)_{\rm rms}$ and E_Y is excellent. The prediction of the pitching angle is not as good as that of the plunging displacement, even though the behavior of the near-aerodynamic and structural resonance is again reproduced correctly. The BEM manages to replicate the near-structural resonance and the near-aerodynamic resonance behavior for both $(Y/c)_{\rm rms}$ and E_Y. A phase plot of Y/c at $f_s = 54.7$ Hz is given in Fig. 12. It clearly shows the near-resonance behavior of Y/c. In view of these results, the BEM, although formulated assuming two-dimensional inviscid flow and hence no vorticity diffusion, can replicate the phenomenon of fluid–airfoil interaction in a real flow with finite Reynolds number fairly correctly. This is evidence of the range of applicability of the BEM.

IV. Conclusions

An experiment has been devised whereby two parallel rows of vortices are superposed on a uniform stream with an airfoil placed symmetrically between the two rows of vortices. The experiment was set up to investigate the structural and aerodynamic response of the airfoil resulting from fluid–airfoil interaction due to excitation created by the oncoming vortices. The two rows of vortices were produced by placing two identical cylinders in a side-by-side arrangement at a fixed distance ahead of the leading edge of the airfoil with chord length c. The flow Reynolds number varied from $\sim 8 \times 10^4$ to around 2×10^5. Because it was difficult to ensure that the two KVSs thus produced were identical and synchronized, there was a time lag (or lead) between the two rows of shed vortices. This time lag was equivalent to releasing the vortices from the cylinders at a separation distance x_r. Furthermore, the vortex separation distance d could be varied by changing the cylinder diameter at a fixed freestream velocity. These two changes allow the effect of changing d and x_r to be investigated. Six different cylinder arrangements were studied and this gave rise to six different excitation frequencies and six different values for x_r.

The measured plunging displacement and pitching angle of the airfoil shows that structural resonance occurs when the excitation frequency approaches the bending natural frequency of the airfoil. Furthermore, near-aerodynamic resonance occurs as d approaches

$2c$. The experiment failed to get to this condition but was able to achieve the condition $d = 1.87c$. At this condition, the power spectral density plot shows a very distinct peak at the excitation frequency, thus lending evidence that the response is close to aerodynamic resonance.

The wake behind the two side-by-side cylinders was measured using hot wires. These measurements yielded the wake pattern and the vortex convection velocity. Thus determined, these wake parameters were used as inputs to a BEM technique developed to calculate vortex–blade interaction. The BEM was able to replicate both the structural resonance response and the near-aerodynamic resonance response of the airfoil. This shows that an inviscid formulation based on the Euler equation for the flowfield and a 2-DOF model for the structural dynamics was sufficient to reproduce the fluid–airfoil interaction behavior fairly correctly.

Acknowledgments

Support given by the Research Grants Council of the Government of the HKSAR under Grants PolyU 5128/98E and PolyU 5161/00E is gratefully acknowledged.

References

[1]Fung, Y. C., *The Theory of Aeroelasticity*, Wiley, New York, 1955.

[2]Blevins, R. D., *Flow-Induced Vibration*, 2nd ed., Van Nostrand Reinhold, New York, 1990.

[3]Srinivasan, A. V., "Flutter and Resonant Vibration Characteristics of Engine Blades," *Journal of Fluids Engineering*, Vol. 119, 1997, pp. 742–775.

[4]Hall, K. C., "Eigenanalysis of Unsteady Flows About Airfoils, Cascades, and Wings," *AIAA Journal*, Vol. 32, 1994, pp. 2426–2432.

[5]Jadic, I., So, R. M. C., and Mignolet, M. P., "Analysis of Fluid–Structure Interactions Using a Time-Marching Technique," *Journal of Fluids and Structures*, Vol. 12, 1998, pp. 631–654.

[6]So, R. M. C., Jadic, I., and Mignolet, M. P., "Fluid–Structure Resonance Produced by Oncoming Alternating Vortices," *Journal of Fluids and Structures*, Vol. 13, 1999, pp. 519–548.

[7]Lau, Y. L., Leung, R. C. K., and So, R. M. C., "Wake-Induced Vibration and Its Role in Fatigue Life Estimate of Turbine Blades," *Journal of Turbomachinery* (submitted for publication).

[8]Zdravkovich, M. M., *Flow Around Circular Cylinder*, Vol. 1, Oxford Univ. Press, Oxford, 1997.

[9]Gerrard, J. H., "Numerical Computation of the Magnitude and Frequency of the Lift on a Circular Cylinder," *Philosophical Transactions of the Royal Society of London, Series A: Mathematical and Physical Sciences*, Vol. 216, 1967, pp. 137–162.

[10]Perry, A. E., Chong, M. S., and Lim, T. T., "The Vortex-Shedding Process Behind Two-Dimensional Bluff Bodies," *Journal of Fluid Mechanics*, Vol. 116, 1982, pp. 77–90.

[11]Nakagawa, T., "A Formation Mechanism of Alternating Vortices Behind a Circular Cylinder at High Reynolds Number," *Journal of Wind Engineering and Industrial Aerodynamics*, Vol. 25, 1986, pp. 113–129.

[12]Roshko, A., "On the Wake and Drag of Bluff Bodies," *Journal of the Aeronautical Sciences*, Vol. 22, 1955, pp. 124–132.

[13]Nakagawa, T., Meier, G. E. A., Timm, R., and Lent, H. M., "Influence of Shape on Vortex Shedding from Two-Dimensional Cylinders at High Reynolds Number and High Subsonic Mach Number," Max-Planck-Instiut für Strömungsforschung, Bericht 22, Göttingen, Germany, 1985.

[14]Gerrard, J. H., "The Mechanics of the Formation Region of Vortices Behind Bluff Bodies," *Journal of Fluid Mechanics*, Vol. 25, 1966, pp. 401–413.

[15]Schaefer, J. W., and Eskinazi, S., "An Analysis of the Vortex Street Generated in a Viscous Fluid," *Journal of Fluid Mechanics*, Vol. 6, 1959, pp. 241–259.

[16]Bearman, P. W., "Investigation of the Flow Behind a Two Dimensional Model with a Blunt Trailing Edge and Fitted with Splitter Plates," *Journal of Fluid Mechanics*, Vol. 21, 1965, pp. 241–255.

[17]Griffin, O. M., "Effect of Synchronized Cylinder Vibration on Vortex Formation and Mean Flow," *Proceedings of the Flow-Induced Structural Vibrations, IUTAM/IAHR Symposium*, Springer-Verlag, Berlin, 1972, pp. 454–470.

[18]Ozono, S., "Flow Control of Vortex Shedding by a Short Splitter Plate Asymmetrically Arranged Downstream of a Cylinder," *Physics of Fluids*, Vol. 11, No. 10, 1999, pp. 2928–2934.

[19]Hasan, M. A. Z., and Budair, M. O., "Role of Splitter Plates in Modifying Cylinder Wake Flows," *AIAA Journal*, Vol. 32, No. 10, 1994, pp. 1992–1998.

[20]Nakagawa, T., Meier, G. E. A., Timm, R., and Lent, H. M., "Vortex Shedding of a Square Cylinder in Front of a Slender Airfoil at High Reynolds Number. Part 1: Spacing Effect," Max-Planck-Instiut für Strömungsforschung, Bericht 23, Göttingen, Germany, 1985.

[21]Lau, Y. L., So, R. M. C., and Leung, R. C. K., "Wake-Induced Vibration of Elastic Slender Structures," *Journal of Fluids and Structures* (submitted for publication).

[22]Zdravkovich, M. M., "Review of Flow Interference Between Two Circular Cylinders in Various Arrangements," *Journal of Fluids Engineering*, Vol. 99, 1977, pp. 618–633.

[23]Landweber, L., "Flow About a Pair of Adjacent, Parallel Cylinders Normal to a Stream," D. W. Taylor Model Basin, Dept. of the Navy, Rept. 485, Washington, DC, 1942.

[24]Spivac, H. M., "Vortex Frequency and Flow Pattern in the Wake of Two Parallel Cylinders at Varied Spacings Normal to an Air Stream," *Journal of the Aeronautical Sciences*, Vol. 13, 1946, pp. 289–297.

[25]Ishigai, S., Nishikawa, E., Nishmura, K., and Cho, K., "Experimental Study on Structure of Gas Flow in Tube Banks with Tube Axes Normal to Flow (Part 1: Karman Vortex Flow Around Two Tubes at Various Spacings)," *Bulletin of the Japan Society of Mechanical Engineers*, Vol. 15, 1972, pp. 949–956.

[26]Zhang, H. J., Zhou, Y., So, R. M. C., Mignolet, M. P., and Wang, Z. J., "A Brief Note on the Damping of an Elastic Cylinder in a Cross Flow," *Journal of Fluids and Structures*, Vol. 17, 2003, pp. 479–483.

[27]Baban, F., So, R. M. C., and Ötugen, M. V., "Unsteady Forces on Circular Cylinders in a Cross Flow," *Experiments in Fluids*, Vol. 7, 1989, pp. 293–302.

[28]So, R. M. C., Zhou, Y., and Liu, M. H., "Free Vibrations of an Elastic Cylinder in a Cross Flow and Their Effects on the Near Wake," *Experiments in Fluids*, Vol. 29, No. 2, 2000, pp. 130–144.

[29]So, R. M. C., Liu, Y., Chan, S. T., and Lam, K., "Numerical Studies of a Freely Vibrating Cylinder in a Cross Flow," *Journal of Fluids and Structures*, Vol. 15, No. 7, 2001, pp. 845–866.

[30]Chen, Y. N., "Fluctuating Lift Forces of the Karman Vortex Streets on a Single Circular Cylinder and in Tube Bundle. Part 1—The Vortex Street Geometry of the Single Circular Cylinder," *Journal of Engineering for Industry*, Vol. 94, No. 2, 1971, pp. 603–628.

[31]Chorin, A. J., "Numerical Study of Slightly Viscous Flow," *Journal of Fluid Mechanics*, Vol. 57, 1973, pp. 785–796.

[32]Yao, Z. X., and Liu, D. D., "Vortex Dynamics of Blade–Blade Interaction," AIAA Paper 94-0737, Jan. 1994.

[33]Yao, Z. X., Garcia-Fogeda, P., Liu, D. D., and Shen, G., "Vortex/Wake Flow Studies for Airfoils in Unsteady Motions," AIAA Paper 89-2225, July–Aug. 1989.

M. Ahmadian
Associate Editor